

Behavior of CFST columns with inner CFRP tube under biaxial eccentric loading

Guochang Li^{1a}, Zhijain Yang^{*1}, Yan Lang^{2b} and Chen Fang^{3c}

¹ School of Civil Engineering, Shenyang Jianzhu University, Shenyang, 110168, China

² Department of Building Engineering, Suqian College, Jiangsu Province, 223800, China

³ Department of Civil Engineering, University of Texas at El Paso, El Paso, TX 79968, USA

(Received May 25, 2016, Revised November 05, 2016, Accepted December 02, 2016)

Abstract. This paper presents the results of an experimental study on the behavior of a new type of composite FRP-concrete-steel member subjected to bi-axial eccentric loading. This new type of composite member is in the form of concrete-filled square steel tube slender columns with inner CFRP (carbon fiber-reinforced polymer) circular tube, composed of an inner CFRP tube and an outer steel tube with concrete filled in the two tubes. Tests on twenty-six specimens of high strength concrete-filled square steel tube columns with inner CFRP circular tube columns (HCFST-CFRP) were carried out. The parameters changed in the experiments include the slenderness ratio, eccentric ratio, concrete strength, steel ratio and CFRP ratio. The experimental results showed that the failure mode of HCFST-CFRP was similar to that of HCFST, and the specimens failed by local buckling because of the increase of lateral deflection. The steel tube and the CFRP worked together well before failure under bi-axial eccentric loading. Ductility of HCFST-CFRP was better than that of HCFST. The ultimate bearing capacity of test specimen was calculated with simplified formula, which agreed well with test results, and the simplified formula can be used to calculate the bearing capacity of HCFSTF within the parameters of this test.

Keywords: CFRP tube; high strength concrete-filled square steel tube; bi-axial eccentric; slenderness ratio; slender column

1. Introduction

High strength concrete has become more economic and readily available, and its stiffness and strength are greater than conventional strength concrete. The weakness of high strength concrete is its fragility. An effective way to improve the above problem is to fill it in steel tube (Lue *et al.* 2007, Yang *et al.* 2008, Fan *et al.* 2009, Zhu *et al.* 2010). The high strength concrete-filled square steel tubular column (HCFST) has many advantages compared with the ordinary steel or reinforced concrete column due to its high-strength, stiffness, durability, ductility and better seismic resistance. On the other hand, it also has unique characteristics: (1) simple form of beam-to-column connection; (2) flexible building layout; (3) good stability behavior with large cross-

*Corresponding author, Ph.D., E-mail: faemail@163.com

^a Professor, E-mail: liguochang0604@sina.com

^b Ph.D. Student, E-mail: llangyan@163.com

^c Ph.D. Student, E-mail: chenleofang@gail.com

section moment of inertia; (4) convenient construction. Thus, HCFST columns have been widely applied in high-rise buildings.

In recent years, fiber reinforced polymer (FRP) composites are becoming a widely accepted technology in the construction industry because of their well-known advantages such as high ratio of strength-to-weight and good corrosion resistance. Many experimental studies have been conducted to examine the performance of FRP composites in retrofitting existing concrete columns (e.g., Lam and Teng 2003, Fam *et al.* 2005, Ozbakkaloglu and Saatcioglu 2006, Matthys *et al.* 2006, Ozbakkaloglu and Oehlers 2008, Ozbakkaloglu and Akin 2011, Ozbakkaloglu 2012, Ozbakkaloglu and Vincent 2013). FRP combined with concrete filled steel tube has become increasingly popular. Numerous research has explored the behavior of the composite columns, the results show that the advantages of the FRP, steel tube and concrete are fully played (Yu *et al.* 2006, Han *et al.* 2010, Yu and Teng 2012, Yu *et al.* 2012, 2014, Ozbakkaloglu and Fanggi 2013, Albitar *et al.* 2014, Zhang *et al.* 2014, 2015, Fanggi and Ozbakkaloglu 2015a, b, Idris and Ozbakkaloglu 2016).

The concrete-filled square steel tube could not perform as well as a circular one because a square steel tube provides less confinement and the constraint of concrete filled steel tube is mainly in the corner. Local buckling is easy to happen in the square steel tube. Therefore, high concrete-filled square steel tube columns with inner CFRP circular tube column (referred to as HCFST-CFRP column) is a new form of composite column that was put forward to improve constraint behavior of square steel tube by Li and Ma (2009). A CFST-CFRP column consists of core concrete, sandwiched concrete between an outer tube made of steel and an inner tube made of CFRP, as shown in Fig. 1. Li *et al.* (Li and Ma 2009, Li and Li 2011, Li *et al.* 2011, 2013a) has reported the tests on HCFST-CFRP columns under concentric loading. The results showed that carrying capacity of the composite member could be improved. Li *et al.* (Li and Yang 2009, Li *et al.* 2013b) conducted tests on HCFST-CFRP columns subjected to eccentric loading and pure bending, it has been found that CFRP and steel tube could work well together.

The corner columns in buildings which are subjected to lateral loads tend to be biaxial bending. It is necessary to study the performance of such columns, and some achievements have been made about HCFST columns. Bridge (1976) studied on four concrete-filled rectangular hollow section steel tubes subjected to bi-axial eccentric loading, and showed that the bearing capacity of the specimen has a close relationship with the eccentric angle. Mursi and Uy (2006a) conducted test on hollow and concrete filled steel columns fabricated with high strength structural steel and subjected to biaxial bending. Mursi and Uy (2006b) presented a numerical model to consider the coupled effect of local and global buckling under biaxial conditions. Li *et al.* (2010) tested on the behavior of square steel tube columns filled with high-strength concrete considering the

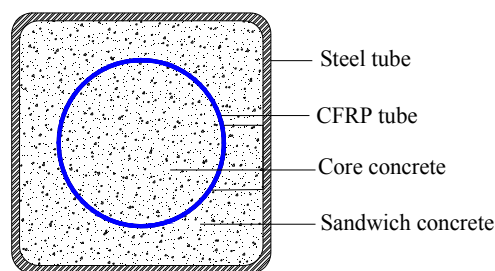


Fig. 1 Cross section of HCFST-CFRP column

slenderness ratio and steel ratio. Guo *et al.* (2011, 2012) studied concrete-filled rectangular steel hollow structural section (HSS) columns formed by slender plates with large depth-to-width ratio subjected to bi-axial bending, and the results showed that local buckling of steel plate appeared after the specimen reached the ultimate capacity. Liang *et al.* (2012) and Patel *et al.* (2015) presented a new multiscale model for bi-axially loaded CFST slender beam-columns which accounted for the effects of local buckling and high strength materials. Idris and Ozbakkaloglu (2016) conducted test on six square FRP–HSC–steel DSTCs under axial and cyclic lateral loading, the test result showed that square DSTCs exhibited ductile behavior under combined axial compression and cyclic lateral load.

The main objective of this paper is to investigate the behavior of high strength concrete-filled square steel tube columns with inner CFRP circular tube (HCFST-CFRP) subjected to bi-axial eccentric loading.

2. Experiment

2.1 Short HCFSTF column test series

The experimental program consisted of fabricating, construction and testing fourteen HCFST-CFRP columns. The parameters of the specimens were steel ratio, eccentric ratio, concrete strength and CFRP ratio. The steel tube was fabricated by cold-rolling steel type Q235. The length of the specimens was 600 mm, cross section of outer steel tube was 200 mm × 200 mm and the diameter of the inner CFRP tube was 125mm. According to specification of EC4, AII and DL/T5085-1999, as the slenderness ratio $\lambda \leq 16$, $L/B \leq 4$ or $L/B \leq 3.5$ respectively, the columns can be defined as short column. All columns had a length to depth ratio (L/B) of 3. The details of specimens are listed in Table 1.

Table 1 Details for the testing of short column

NO.	Specimen	$B \times t$ (mm)	L (mm)	α	β	e/r	ζ_s	ζ_f	f_{cu} (MPa)	N_{ue} (kN)
1	ES40	200×4	600	0.0739	0	0.5	0.290	0	124.6	2105
2	ES41	200×4	600	0.0739	0.0027	0.5	0.290	0.127	124.6	2089
3	ES42	200×4	600	0.0739	0.0054	0.5	0.290	0.254	124.6	2061
4	ES50	200×5	600	0.0965	0	0.5	0.377	0	124.6	2319
5	ES51	200×5	600	0.0965	0.0027	0.5	0.377	0.127	124.6	2178
6	ES52	200×5	600	0.0965	0.0054	0.5	0.377	0.254	124.6	2236
7	ES60	200×6	600	0.1269	0	0.5	0.540	0	124.6	2283
8	ES61	200×6	600	0.1269	0.0027	0.5	0.540	0.127	124.6	2334
9	ES62	200×6	600	0.1269	0.0054	0.5	0.540	0.254	124.6	2245
10	ES52-1	200×5	600	0.0965	0.0054	0.2	0.547	0.387	81.8	2596
11	ES52-2	200×5	600	0.0965	0.0054	0.35	0.547	0.387	81.8	2153
12	ES52-3	200×5	600	0.0965	0.0054	0.5	0.547	0.387	81.8	1580
13	ES52-4	200×5	600	0.0965	0.0054	0.65	0.547	0.387	81.8	1306
14	ES52-5	200×5	600	0.0965	0.0054	0.8	0.547	0.387	81.8	1089

The specimen number (for example: ESF52) in Table 1 are labeled as follows: *E* stands for biaxial eccentricity; *S* stands for steel; *F* stands for CFRP. The first number stands for the thickness of steel tube, as follow: 4, 5 and 6 means 3.5 mm, 4.5 mm and 5.8 mm, respectively. The second number stands for the layers of CFRP which is 0, 1 or 2 layers. *B* is cross section width of steel tube; *t* is the nominal thickness of steel tube; *L* is the length of specimen; α is steel ratio, expressed as $\alpha = A_s/A_c$, where, A_s is area of steel tube and A_c is area of concrete; β is CFRP ratio, expressed as $\beta = A_f/A_c$, where, A_f is area of CFRP tube; e/r is eccentric ratio; ζ_s is steel confinement factor, expressed as $\zeta_s = \alpha(f_y/f_{ck})$, where, f_y is yield strength of steel and f_{ck} is axial compressive strength of concrete ($= 0.4f_{cu}^{7/6}$ presented by Yu (Yu and Ding 2003), where f_{cu} is cubic compressive strength of concrete); ζ_f is CFRP confinement factor, expressed as $\zeta_f = \beta(f_f/f_{ck})$, where f_f is tensile strength of CFRP.

2.2 Material Properties

2.2.1 Compressive strength of concrete

All the specimens were cast with one batch of ready-mixed and self-compacting concrete, and the slump was 180 ± 20 mm. Maximum size of coarse aggregate was 12 mm. To determine the compressive strength of concrete, six $150 \text{ mm} \times 150 \text{ mm} \times 150 \text{ mm}$ cubes were cast and cured in conditions similar to the related specimens. The tests were carried out in accordance with the provisions of GB/T 50081-2002 (2003). Concrete cubes were tested at 28 days and test days. The average cube strength (f_{cu}) of ES40~ES62 and ES52-1~ES52-5 are given in Tables 2 and 3. It is noted that the compressive strength of concrete increases with the age.

Table 2 Concrete compressive strength tests for ES40~ES62

Sample	Age of concrete	f_{cu} (MPa)	Average f_{cu} (MPa)
1		94.7	
2		91	
3	28 days	96	94.3
4		99	
5		91.1	
6		118.5	
7	670 days (Test)	131	124.6
8		123.5	

Table 3 Concrete compressive strength tests for ES52-1~ES52-5

Sample	Age of concrete	f_{cu} (MPa)	Average f_{cu} (MPa)
1		62.4	
2	28 days	64.4	62.7
3		61.2	
4		82.2	
5	97 days (Test)	80.7	81.8
6		82.4	

Table 4 Material property of steel tube

Specimen	f_y (MPa)	Average f_y (MPa)	f_u (MPa)	Average f_u (MPa)	E (GPa)	Average E (GPa)	ν	Average ν
S4-1	307		432		195		0.278	
S4-2	307	306	429	430	206	200	0.293	0.284
S4-3	304		429		198		0.28	
S5-1	286		417		206		0.287	
S5-2	292	291	417	418	186	196	0.306	0.300
S5-3	294		419		195		0.307	
S6-1	306		433		206		0.276	
S6-2	349	333	444	441	212	206	0.281	0.276
S6-3	344		447		200		0.272	

2.3.2 Tensile coupon tests of steel

Three tensile coupon tests for different thickness were conducted to determine the tensile strength of steel. Dimensions were in accordance with Chinese standard GB/T228-2002 (2003). The average yield strength (f_y), ultimate tensile strength (f_u), elastic modulus (E), and Poisson ratio (ν) are listed in Table 4.

2.3.3 Tensile coupon tests of CFRP

Carbon fiber reinforced polymer composite material was selected to fabricate the FRP tube because of the higher elastic modulus and tensile strength, which was believed to be more compatible with high modulus of high strength concrete. Tensile tests on CFRP coupons were conducted according to the Chinese standard GB/T 3354-1999 (2000). The test results are given in Table 5. The values presented were the averages from three test coupons based on a nominal thickness of 0.167 mm/ply. Where f_u is ultimate tensile strength, E is elastic modulus, ϵ_u is the ultimate strain, ν is Poisson ratio.

2.3 Preparation of specimens

The preparation process of the HCFST-CFRP specimen included the following three steps: (1) Prefabricating of CFRP tube (Fig. 2); The CFRP tubes were manufactured from carbon fiber sheets and epoxy resin by manually wrapping impregnated CFRP sheets around polyvinyl chloride (PVC) templates. The CFRP tubes were manufactured by unidirectional carbon fiber sheets with fibers oriented in the hoop direction. The CFRP sheets were wrapped one layer at a time with a

Table 5 Material properties of CFRP

Specimen	f_u (MPa)	Average f_u (MPa)	E (GPa)	Average E (GPa)	ϵ_u (%)	Average ϵ_u	ν	Average ν
F1	3653		287		11881		0.337	
F2	3825	3718	296	292	13681	13678	0.373	0.304
F3	3677		294		15471		0.201	



Fig. 2 Fabrication of CFRP tube

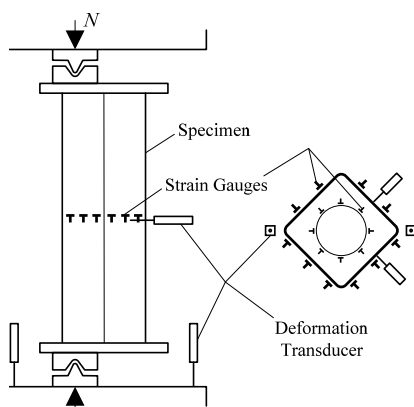


Fig. 3 Assembling of specimen

100 mm overlap in the direction of fibers to ensure proper bond, and overlapped with a 20 mm overlap along the column height. (2) Assembling of the specimen (Fig. 3), which consisted of a steel tube outside, a CFRP tube inside, and the CFRP tube was fixed by iron hoop. (3) Concrete casting.

2.4 Instrumentation, test setup, and loading program

The test setup for the short columns is illustrated in Fig. 4. All of the columns were performed on a 5000 kN capacity testing machine, and the test data were collected by a static data acquisition system. Knife edges were used at two ends of the columns to ensure boundary conditions to be pinned in test. Two linear varying displacement transducers (LVDTs) were used to measure deflections of the column at the mid-height, and two LVDTs were placed near to the corner of the column end plates to record the shortening of the columns tested, as shown in Fig. 4. Twenty strain gauges were mounted on the steel tube surface to measure strains at the mid-height, and sixteen strain gauges were attached to the CFRP tube surface. The locations of strain gauge are shown in Fig. 4.



(a) Diagrammatic test set up



(b) Test photo

Fig. 4 Test setup of short HCFSTF-CFRP column



(a) ES40~ES62 series columns



(b) ES52-1~ES52-5 series columns

Fig. 5 Failure modes of short columns

Preliminary test within the elastic range was conducted to adjust the position of the specimen based on measurements of strain gauges attached at the mid-height of the specimen. A load interval of less than one tenth of the estimated load capacity was used. Each load interval was maintained for three minutes. At each load increment, the strain readings and the deflection measurements were recorded.

2.5 Short HCFST-CFRP column test results

2.5.1 Failure modes

The failure modes of columns are shown in Fig. 5. The deformation increased gradually with the increase of load at initial stage. As reaching its bearing capacity, the local buckling occurred at the compressive face of steel tube near the mid-height.

The typical failure mode of specimen ES52-1 is shown in Fig. 6. After taking off the buckling steel tube, it can be found that the sandwich concrete was seriously crushed (as shown Fig. 6(b)). On the opposite position, the concrete was tensioned to crack (as shown Fig. 6(c)).

After taking off the sandwich concrete, it can be seen that the compressive zone of CFRP tube ruptured in the hoop direction near the mid-height, and there were several cracks at the appropriate position of core concrete (as shown Fig. 6(c)).

2.5.2 Axial load-deflection of short columns

The axial load-deflection relationship curves at the mid-height are shown in Fig. 7. The deflection u_m ($u_m = \sqrt{u_x^2 + u_y^2}$) was calculated by the deflections of u_x (deflection along x axis) and u_y (deflection along y axis) which were registered by LVDTs of mid-height of column. It can be seen that the deflection of specimen was not obvious, and the load was in linear relation with

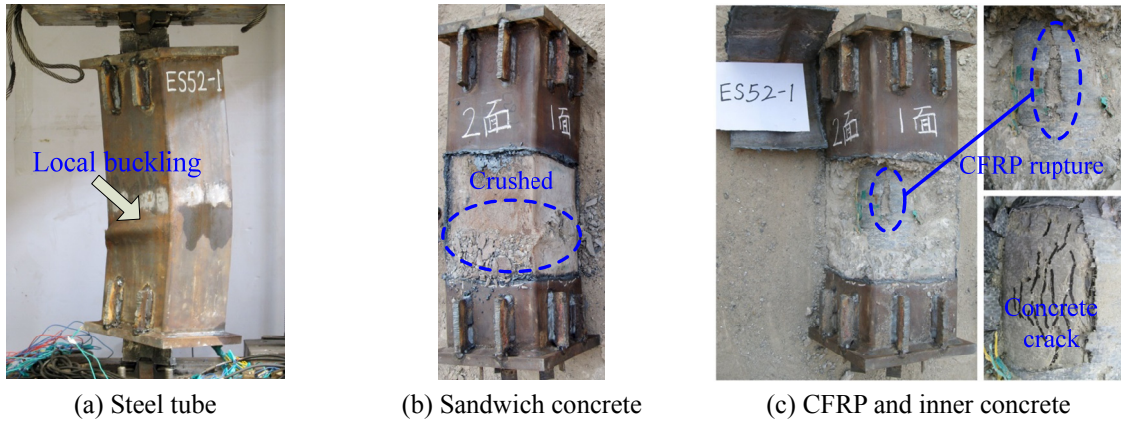


Fig. 6 The failure mode of ES52-1

deflection before load attained about 70% of ultimate bearing capacity. Then, the relation between load and deflection was nonlinear. As the load reached the ultimate bearing capacity, steel tube began to undergo local buckling on the compressive face of specimen, and the continuous cracks appeared at the inner concrete. The bearing capacity descended rapidly until it achieved about 75% ultimate bearing capacity, and local buckling became more apparent. When a violent fracture of CFRP came from the inner of the specimen, the bearing capacity of specimen sharply descended, as shown in Fig. 7(a).

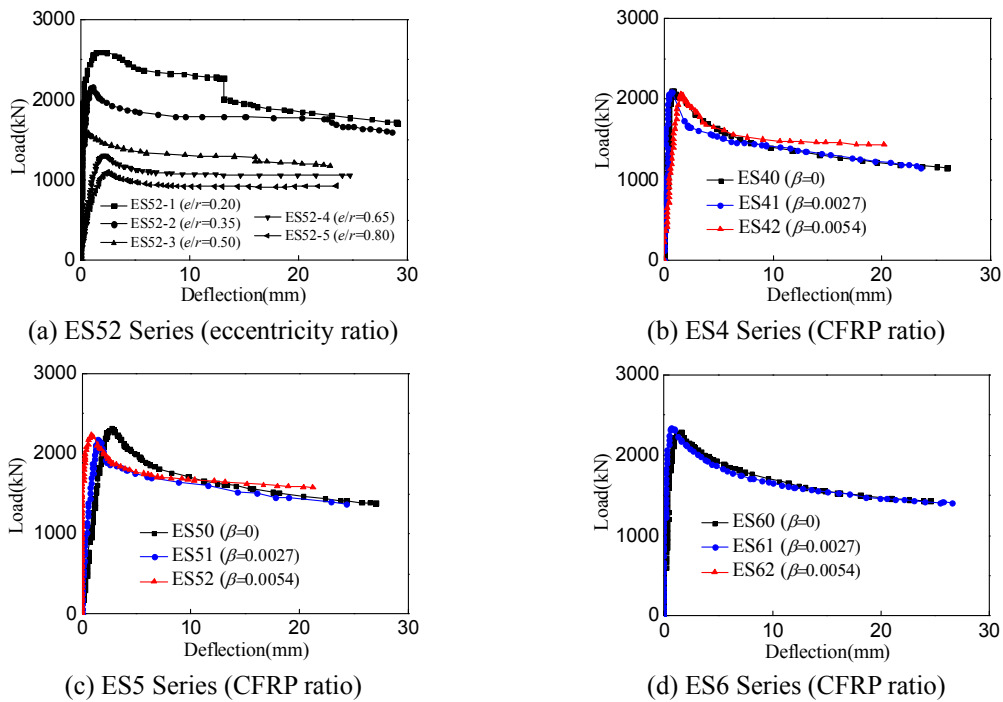


Fig. 7 Axial load (N)-deflection (um) relationship curves of short columns

Fig. 7 indicates the influences of eccentric ratio and CFRP ratio on specimens. HCFST-CFRP short column shows better ductility than HCFST short column. The ductility of HCFST-CFRP short column increases with the thickness of CFRP tube, which means that the CFRP tube can improve the ductility of HCFST column. As illustrated in Fig. 7(a), the ultimate bearing capacity decreases with the increase of eccentric ratio. It can be seen from Figs. 7(b)-(d) that the confinement effect of CFRP tube becomes weakened when the eccentric ratio is too large.

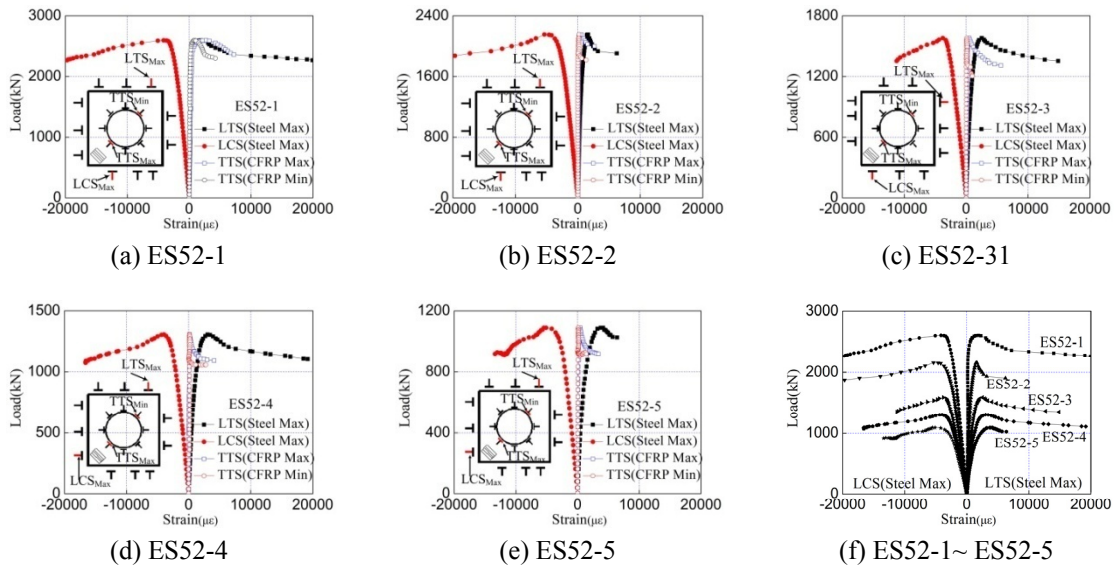


Fig. 8 Load (N) versus Strain (ϵ) Relationship

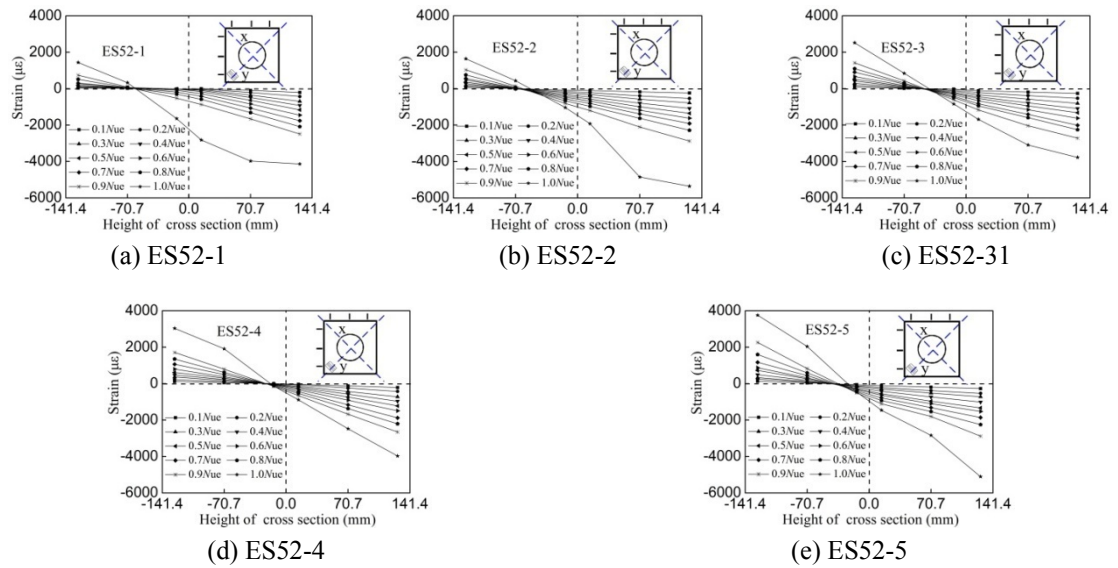


Fig. 9 Strain distribution of specimen ES52-1~ES52-5

Table 6 Details of slender columns

NO.	Specimen number	$B \times t$ (mm)	L (mm)	α	β	e/r	ξ_s	ξ_f	λ	N_{ue} (kN)
1	ESF4-5-28	200×5	800	0.0965	0.0054	0.2	0.547	0.387	13.9	2483
2	ESF4-5-71	200×5	800	0.0965	0.0054	0.5	0.547	0.387	13.9	1761
3	ESF4-5-113	200×5	800	0.0965	0.0054	0.8	0.547	0.387	13.9	1063
4	ESF6-5-28	200×5	1200	0.0965	0.0054	0.2	0.547	0.387	20.8	2618
5	ESF6-5-71	200×5	1200	0.0965	0.0054	0.5	0.547	0.387	20.8	1463
6	ESF6-5-113	200×5	1200	0.0965	0.0054	0.8	0.547	0.387	20.8	1146
7	ESF8-5-28	200×5	1600	0.0965	0.0054	0.2	0.547	0.387	27.7	2417
8	ESF8-5-71	200×5	1600	0.0965	0.0054	0.5	0.547	0.387	27.7	1508
9	ESF8-5-113	200×5	1600	0.0965	0.0054	0.8	0.547	0.387	27.7	1022
10	ESF10-5-28	200×5	2000	0.0965	0.0054	0.2	0.547	0.387	34.6	2346
11	ESF10-5-71	200×5	2000	0.0965	0.0054	0.5	0.547	0.387	34.6	1477
12	ESF10-5-113	200×5	2000	0.0965	0.0054	0.8	0.547	0.387	34.6	1004

2.5.3 Axial load-strains of short columns

The axial load-strain relationship curves of the short columns are shown in Fig. 8, in which LTS is the longitudinal tensile strain, LCS is the longitudinal compressive strain, and TTS is the transverse tensile strain. The positions of the strain gauges are noted in Fig. 8.

It can be found from Fig. 8 that the strains of CFRP and steel didn't develop simultaneously. After steel tube yielded, the strains of CFRP began to grow quickly. The analysis results indicated that CFRP began to affect mechanism of the short column after the bearing capacity of specimen descended. Fig. 8 shows that strain gauge of maximum TTS was at compressive zone, and minimum TTS was in at tensile zone. There is a great different between maximum TTS and minimum TTS, which means that the confinement effect of CFRP tube was reduced as subjected to biaxial eccentric loading. It also illustrated that the maximum TTS and minimum TTS decreased with the increase of eccentric ratio.

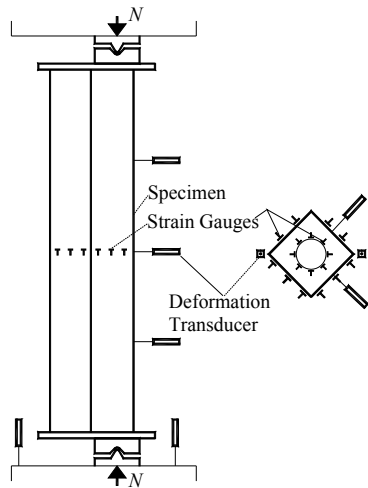
The longitudinal strain distributions of cross section at different load levels are shown in Fig. 9. It can be seen that the strain on the surface remained almost linear along the height of the cross section, which means that the surface remained plane during the loading. The strain near the loading position was negative and increased with the increase of load. The Fig. 9 also shows that the neutral axis moved toward the loading position with the increase of load.

2.6 Slender HCFST-CFST column test series

Twelve slender HCFST-CFRP columns subjected to bi-axial eccentric loading were constructed and tested. The parameters were the eccentric ratio and slenderness ratio. The eccentric ratio along major axis ranged from 0.2 to 0.8, and eccentric angle was 45°. Table 6 gives the details of the specimens. Where, λ is the slenderness ratio. The specimen number (for example:ESF4-5-28) in Table 6 were labeled as follows: letters E stands for bi-axial eccentric load; S stands for steel; F stands for CFRP; 4 stands for length-diameter ratio, $L/B = 4, 6, 8, 10$; 5 stands for the thickness of steel tube; 28 stands for eccentricity: 28 mm, 71 mm, 113 mm. The average

cube strength (f_{cu}) is 81.8 MPa, yield strength is 291 MPa, ultimate tensile strength is 418 MPa.

The test setup is illustrated in Fig. 10. Six LVDTs were used to measure the out-of-plane deflections of the column at the mid-height and quarter points of the column, and two LVDTs were placed near to the end plate of the column to record the shortening of the column, as shown in Fig. 10. The locations of strain gauges are shown in Fig. 10(a).



(a) Diagrammatic test set up



(b) Test photo

Fig. 10 Test setup of slender HCFST-CFST column



Fig. 11 Typical failure mode of medium long column

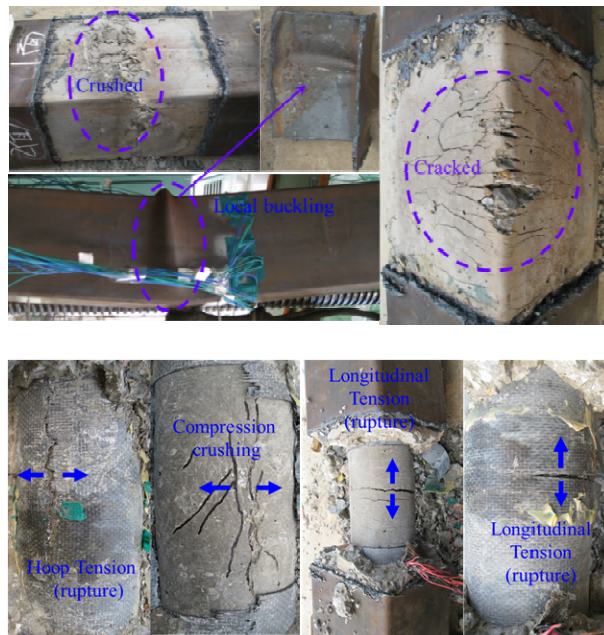


Fig. 12 Failure mode of steel tube, sandwich concrete, the inner CFRP and core concrete

2.6.1 Failure modes

The typical failure mode of columns is illustrated in Fig. 11. It was observed that most of the columns demonstrated global buckling followed by local buckling and behaved in a ductile manner. A few cases were found to be failed in local buckling after the peak load.

In the test, the deflection increased gradually with the increase of load at the initial stage, which was approximately proportional to the load. As the load reached 60%~70% of the ultimate bearing capacity, the deflection started to increase significantly. Due to the influence of second-moment effect, the growth of second-moment was larger than growth of section resistance moment which caused the decrease of bearing capacity and the rapid increase of deflection.

When the load decreased to 85% of the ultimate bearing capacity, the rupture voice of the CFRP tube could be heard. The voice was very clear when the slenderness ratio and eccentricity was small.

After taking off the steel tube, the failure modes of sandwich concrete are shown in Fig. 12. It can be seen that the concrete crushed in the compressive zone, and the steel tube appeared local buckling with the expansion of concrete volume. On the opposite part, the concrete was under tension, and cracks occurred which became smaller from the corner to the web. In addition, the tension area increased with increase of the eccentric ratio. The tensile area was approximately 8%, 15%, and 30% of the concrete cross section when the eccentric ratio was 0.2, 0.5 and 0.8, respectively. According to failure mode of specimens, the number and width of concrete crack in the tensile zone increased with increase of eccentric ratio. The phenomenon indicated that the concrete had emerged tensile stress at the initial stage.

Typical failure mode of inner CFRP tube and core concrete was shown in Fig. 12. The CFRP

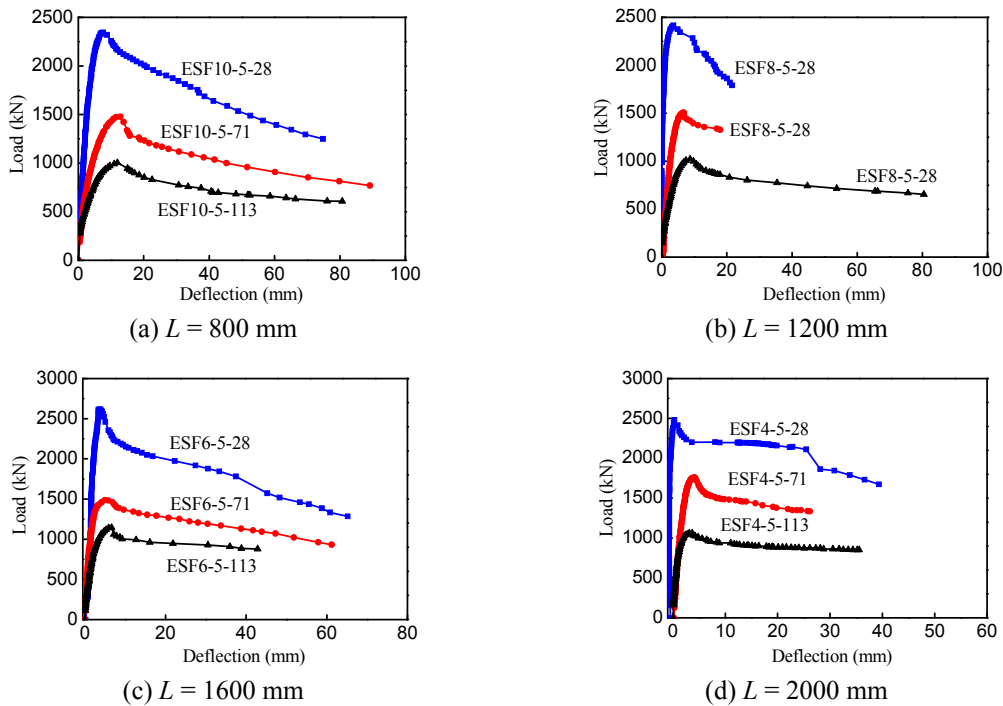


Fig. 13 Axial load (N)-deflection (u_m) relationship curves of slender columns

tube fractured in the hoop direction where the steel tube appeared local buckling. In addition, it was observed that cracks occurred at tensile zone of CFRP tube along longitudinal direction because CFRP tubes were manufactured with unidirectional carbon fiber sheets, and the tensile stresses were sustained by epoxy resin. Additionally, and there were several cracks at the corresponding position of core concrete. It was evident that bond resistance between the CFRP and concrete was desirable. Therefore, the shear strength and normal force can be transferred very well.

As slenderness ratio was constant, the cracks of the CFRP tube and core concrete in the compression zone decreased with the increase of eccentric ratio. On the opposite part, the cracks of the CFRP tube and core concrete increased. The test phenomenon indicated that the constraint effect of CFRP tube was not obvious when the eccentric ratio was too large.

The CFRP tube did not damage because of slippage of overlap. The overlap and bond between different layers are desirable and the CFRP tube could be considered as integrity.

2.6.2 Axial load-deflection of slender columns

The deflection of the column was recorded by displacement transducer. The LVDTs were located perpendicularly to the two adjacent sides of the column in the tensile side. The position of the LVDTs located at the top quarter of the column, mid-height and the bottom quarter of the column as shown in Fig. 10. Fig. 13 illustrated the axial load-deflection curves of the specimens.

2.6.3 Axial load-strain of slender columns

Fig. 14 illustrates the axial load-strains curves of CFRP and steel tube. It can be seen that the development of both longitudinal and lateral strains of the steel tube were almost the same as the

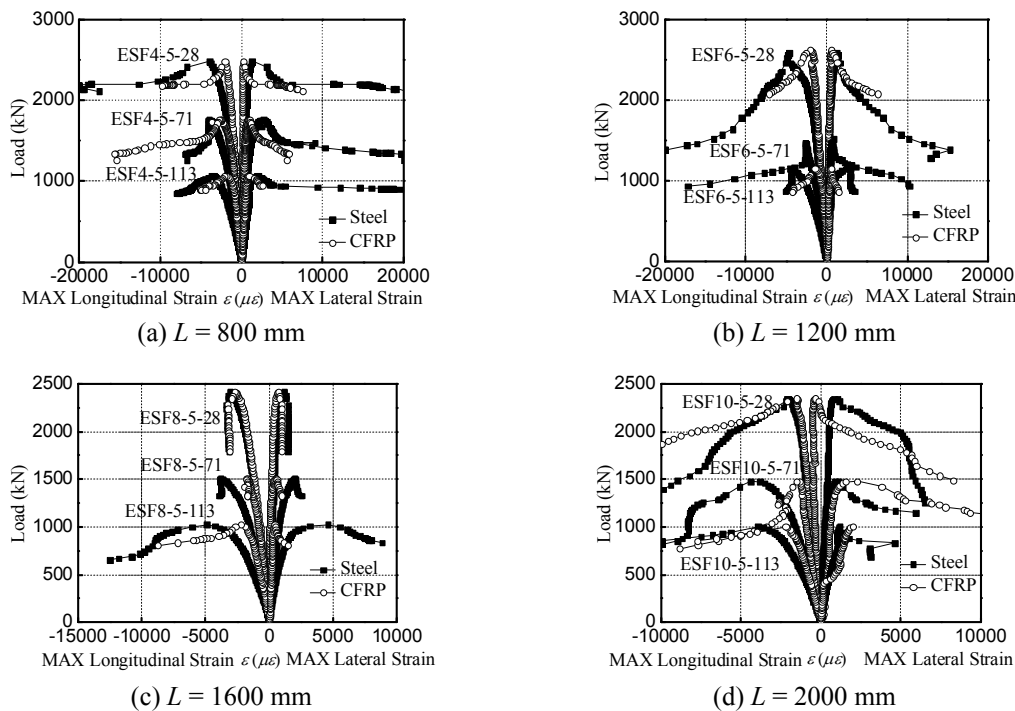


Fig. 14 Axial load versus strain curves for tested specimens

CFRP tube until the tube ruptured. The two components worked together well before the CFRP tube ruptured.

In addition, when the load reached the ultimate bearing capacity, the strain of CFRP started to decrease more significantly than steel, because the ductility of steel tube was better than that of CFRP. The stiffness of the specimen and strain of CFRP decreased with the increase of eccentric ratio and slenderness ratio. It also illustrates that the constraint effectiveness of CFRP tube declined.

2.7 Parameter analysis

2.7.1 Effect of eccentric ratio

Fig. 13 illustrates axial load-deflection curves of the slender columns. When the slenderness ratio was invariant, the stiffness and bearing capacity declined with the increase of eccentric ratio, and deflection of mid-height increased. When the eccentric ratio was 0.2, the load descended significantly after reached the ultimate bearing capacity and lasted for a short time, but the deflection was small. Otherwise, when the load descended to 90% of the ultimate bearing capacity, the load decreased slowly, and the deflection increased quickly. When the eccentric ratio was 0.5, the slope of load-deflection curve was small after the ultimate bearing capacity, and the curve nearly maintained horizontal. In addition, the slenderness ratio and eccentric ratio have significant influences on the confinement effect of CFRP tube. CFRP tube can enhance the bearing capacity and stiffness of the specimens effectively as the eccentric ratio was small, whereas the enhancement was not significant for large eccentric ratio.

2.7.2 Effect of slenderness ratio

Fig. 15 shows the curves of load versus deflection of different slenderness ratio. When the eccentric distance was the same, the ultimate load and stiffness decreased with the slenderness ratio increase.

2.7.3 Effect of steel ratio

Fig. 16 shows the curves of load versus deflection of different steel ratio. With a constant eccentricity ratio and the steel ratio changing from 7% to 13%, the ultimate bearing capacity and stiffness increased. It shows that steel ratio is an important factor to influence ultimate bearing capacity.

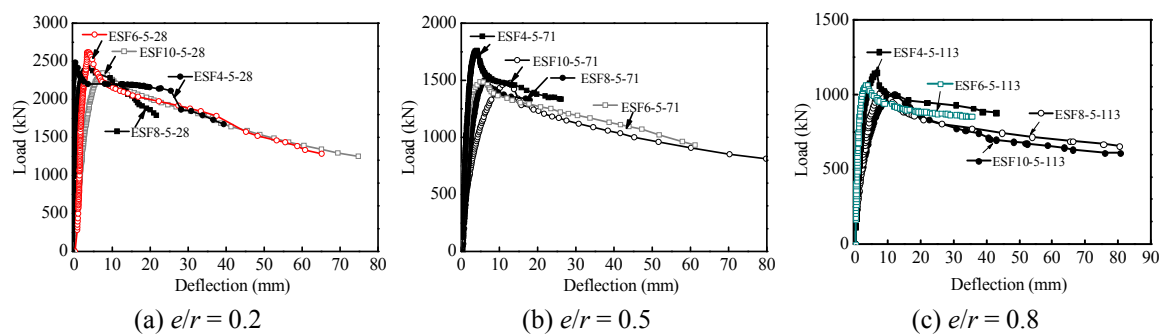


Fig. 15 Effect of slenderness ratio on load versus deflection curves of columns

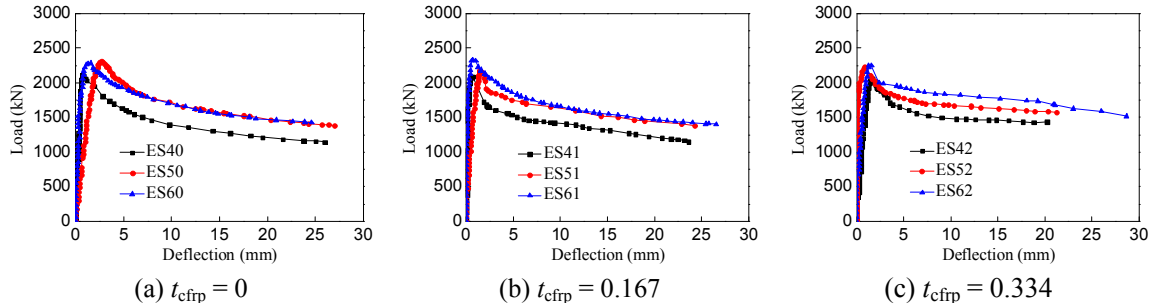


Fig. 16 Effect of steel ratio on load versus deflection curves of columns

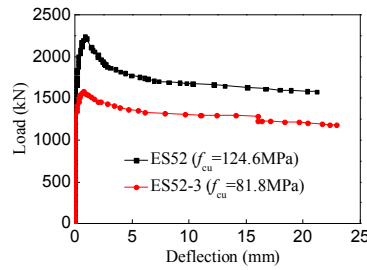


Fig. 17 Effect of concrete strength on load versus deflection curves of columns

2.7.4 Effect of CFRP ratio

Figs. 7(b)-(d) shows the curves of load versus deflection of different CFRP ratio. When the nominal thickness of CFRP tube is 0.167 mm, the ultimate bearing capacity and stiffness can be improved slightly, which is not obvious. When the nominal thickness of CFRP tube is 0.334 mm, the ultimate bearing capacity and stiffness can be improved effectively. It also illustrated that the inner CFRP can improve the ductility.

2.7.5 Effect of concrete strength

Fig. 17 shows the curves of load versus deflection of different concrete strength. It can be observed that the ultimate bearing capacity increased with the increase of concrete strength. Otherwise, the ductility became worse with the increase of concrete strength. It is noted that the high strength concrete can be well confined by steel tube and CFRP.

3. Calculations of ultimate bearing capacity

What is analyzed above shows that the mechanical behavior of HCFST-CFRP is similar with that of HCFST. The interaction equations of $N/N_u - M/M_u$ for HCFST are provided by (Han 2008), and the interaction equations of $N/N_u - M/M_u$ for HCFST-CFRP can be also divided into two parts, which are expressed as follows:

① For $N/N_u \geq \varphi_{xy}^3 2\eta_0$,

$$\frac{N}{\varphi_{xy} N_u} + \frac{a}{d} \left[\left(\frac{M_x}{M_{ux}} \right)^{1.8} + \left(\frac{M_y}{M_{uy}} \right)^{1.8} \right]^{1/1.8} \leq 1 \quad (1)$$

Table 7 Test results and calculation results

NO.	Specimen	N_{ue} (kN)	N_{uc} (kN)	N_{uc}/N_{ue}	Specimen	N_{ue} (kN)	N_{uc} (kN)	N_{uc}/N_{ue}
1	ES40	2105	1506	0.72	ESF4-5-28	2483	2793	1.125
2	ES41	2089	1924	0.92	ESF4-5-71	1761	1608	0.914
3	ES42	2061	2234	1.08	ESF4-5-113	1063	1155	1.086
4	ES50	2319	1983	0.86	ESF6-5-28	2618	2731	1.043
5	ES51	2178	2186	1.00	ESF6-5-71	1463	1559	1.065
6	ES52	2236	2348	1.05	ESF6-5-113	1146	1109	0.967
7	ES60	2283	2580	1.13	ESF8-5-28	2417	2661	1.101
8	ES61	2334	2628	1.13	ESF8-5-71	1508	1454	0.965
9	ES62	2245	2673	1.19	ESF8-5-113	1022	1058	1.035
10	ES52-1	2596	2522	0.97	ESF10-5-28	2346	2586	1.102
11	ES52-2	2153	2074	0.96	ESF10-5-71	1477	1356	0.918
12	ES52-3	1580	1761	1.11	ESF10-5-113	1004	1007	1.003
13	ES52-4	1306	1531	1.17				

② For $N/N_u < 2\varphi_{xy}^3\eta_0$,

$$-b\frac{N^2}{N_u^2} - c\frac{N}{N_u} + \frac{1}{d}\left[\left(\frac{M_x}{M_{ux}}\right)^{1.8} + \left(\frac{M_y}{M_{uy}}\right)^{1.8}\right]^{1/1.8} \leq 1 \quad (2)$$

$$\text{Where } a = 1 - 2\eta_0, \quad b = \frac{1 - \zeta_0}{\eta_0^2}, \quad c = \frac{2(\zeta_0 - 1)}{\eta_0}.$$

Where N_u is ultimate axial bearing capacity of HCFST-CFRP column; φ_{xy} is stability coefficient of CFST under bi-axial eccentric loading; M_x and M_y are bending moment along the x-axis and y-axis respectively, which are given by $M_x = Ne_x$ and $M_y = Ne_y$; M_{ux} and M_{uy} are flexural bearing capacity along the x-axis and y-axis respectively; Where a, b, c, d are calculating coefficients, 1/d is amplification factor of the bending moment considering the second-order effect. The detailed calculations of these parameters are given by Yang (2010).

The stability bearing capacity of test specimen was calculated with the above simplified formula. Table 7 shows calculation results (N_{uc}) and test values (N_{ue}). The ratio of N_{uc}/N_{ue} is listed in Table 8, and the average is 1.03, standard deviation is 0.113. The calculation results agree well with test data, and the simplified formula can be referred to calculate the bearing capacity of HCFSTF within the parameters of this test.

4. Conclusions

This paper has presented and interpreted the results of HCFST-CFRP columns subjected to bi-axial eccentric loading. A HCFST-CFRP is composed of a CFRP inner tube, a steel outer tube, and concrete infill the two tubes. The main parameters examined in this study include the slenderness ratio, eccentric ratio, CFRP and steel ratio. Based on the test results, the following conclusions can be drawn:

- The experimental results shows that the mechanical behavior of HCFST-CFRP and HCFST are similarity due to the increase of deflection, and finally the specimens quit working with strength failure.
- The mechanical properties of inner concrete are improved by CFRP, then longitudinal stress distribution of core concrete and sandwich concrete are discontinuous. Ductility of HCFST-CFRP columns is better than HCFST.
- Confinement effect of CFRP tube to innermost concrete mainly begins to take effect after buckling of steel tube. This is due to enhancement of ductility of HCFST-CFRP column.
- The stiffness and bearing capacity of the specimen decreases with the increase of eccentric ratio, and slenderness ratio. The steel ratio is an important factor to influence ultimate bearing capacity.
- The test results indicated that when eccentric ratio is too large, constraint effect of CFRP tube is not obvious. According to the analysis of load versus strain curves, the two components of CFRP and steel worked together well subjected to bi-axial eccentric loading before the CFRP tube ruptured.
- The formula is suited and safe to calculate the ultimate bearing capacity of HCFST-CFRP column under biaxial eccentric compression.

Acknowledgments

This project was supported by National Science Foundation of China (5157082947), Innovative Research Team of Higher Education in Liaoning Province (LT2014012), Shenyang Engineering and Technological Research Center for Civil Steel Construction Industrialization (F16-076-8-00).

References

- Albitar, M., Ozbakkaloglu, T. and Louk Fanggi, B.A. (2014), "Behavior of FRP-HSC-steel double-skin tubular columns under cyclic axial compression", *J. Compos. Construct.*, **19**(2), 04014041.
- Bridge, R.Q. (1976), "Concrete Filled Steel Tubular Columns Report", No. 8283; School of Civil Engineering, University, Sydney, Australia.
- Fan, H., Li, Q.S., Tuan, A.Y. and Xu, L. (2009), "Seismic analysis of the world's tallest building", *J. Construct. Steel Res.*, **65**(5), 1206-1215.
- Fam, A., Schnerch, D. and Rizkalla, S. (2005), "Rectangular filament-wound glass fiber reinforced polymer tubes filled with concrete under flexural and axial loading: experimental investigation", *J. Compos. Construct.*, **9**(1), 25-33.
- Fanggi, B.A.L. and Ozbakkaloglu, T. (2015a), "Behavior of hollow and concrete-filled FRP-HSC and FRP-HSC-steel composite columns subjected to concentric compression", *Adv. Struct. Eng.*, **18**(5), 715-738.
- Fanggi, B.A.L. and Ozbakkaloglu, T. (2015b), "Square FRP-HSC-steel composite columns: Behavior under axial compression", *Eng. Struct.*, **92**, 156-171.
- Guo, L.H., Zhang, S.M. and Xu, Z. (2011), "Behaviour of filled rectangular steel HSS composite columns under bi-axial bending", *Adv. Struct. Eng.*, **14**(2), 295-306.
- Guo, L.H., Wang, Y.Y. and Zhang, S.M. (2012), "Experimental study of concrete-filled rectangular HSS columns subjected to biaxial bending", *Adv. Struct. Eng.*, **15**(8), 1329-1344.
- GB/T 50081-2002 (2003), Standard for Test Method of Mechanical Properties on Ordinary Concrete; Beijing, China.
- GB/T228-2002 (2003), Metallic Materials-Tensile Testing-Part 1: Method of Test at Room Temperature; Beijing, China.

- GB/T 3354-1999 (2000), Test Method for Tensile Properties of Oriented Fiber Reinforced Plastics; Beijing, China.
- Han, L.H. (2008), *Concrete-Filled Steel Tube Structure-Theory and Practice*, (2nd Edition), Science Press, Beijing, China.
- Han, L.H., Tao, Z., Liao, F.Y. and Xu, Y. (2010), "Tests on cyclic performance of FRP-concrete-steel double-skin tubular columns", *Thin-Wall. Struct.*, **48**(6), 430-439.
- Idris, Y. and Ozbakkaloglu, T. (2016), "Behavior of square fiber reinforced polymer-high-strength concrete-steel double-skin tubular columns under combined axial compression and reversed-cyclic lateral loading", *Eng. Struct.res*, **118**, 307-319.
- Lam, L. and Teng, J.G. (2003), "Design-oriented stress-strain model for FRP-confined concrete", *Construct. Build. Mater.*, **17**(6), 471-489.
- Li, G.C. and Li, S.J. (2011), "Nonlinear finite element analysis on short columns of high strength concrete filled square steel tube with inner CFRP circular tube", *Proceedings of the 7th Conference on Steel and Aluminum Structure*, Kuala Lumpur, Malaysia, August.
- Li, G.C. and Ma, L. (2009), "Experimental study on short columns of high-strength concrete filled square steel tubular with inner CFRP circular tubular under axially compressive load", *Proceedings of International Symposium on Innovation & Sustainability of Structures in Civil Engineering*, Guangzhou, China, November.
- Li, G.C. and Yang, Y. (2009), "Experimental study on high-strength concrete filled square steel tubular beam with inner CFRP circular tube", *Proceedings of the 9th International Conference on Steel Concrete Composite and Hybrid Structures*, Leeds, England, July.
- Li, G.C., Lang, Y. and Yang, Z.J. (2011), "Behavior of high strength CFSST stub columns with inner CFRP tube under axial compressive load", *Adv. Steel Construct.*, **7**(3), 239-254.
- Li, G.C., Yang, Z.J. and Lang, Y. (2010), "Experimental behavior of high strength concrete-filled square steel tube under bi-axial eccentric loading", *Adv. Steel Construct.*, **6**(4), 963-975.
- Li, G.C., Di, C.Y., Tian L. and Fang, C. (2013a), "Nonlinear finite element analysis on long columns of high-strength concrete-filled square steel tube with inner CFRP circular tube under axial load", *Adv. Steel Construct.*, **9**(2), 124-138.
- Li, G.C., Yang, Z.J. and Lang, Y. (2013b), "Behavior of high strength concrete filled square steel tube columns with inner CFRP circular tube under bi-axial eccentric loading", *Adv. Steel Construct.*, **9**(3), 214-229.
- Liang, Q.Q., Patel V.I. and Hadi, M.N. (2012), "Biaxially loaded high-strength concrete-filled steel tubular slender beam-columns, Part I: Multiscale simulation", *J. Construct. Steel Res.*, **75**, 64-71.
- Lue, D.M., Liu, J.L. and Yen, T. (2007), "Experimental study on rectangular CFT columns with high-strength concrete", *J. Construct. Steel Res.*, **63**(1), 37-44.
- Mathys, S., Toutanji, H. and Taerwe, L. (2006), "Stress-strain behavior of large-scale circular columns confined with FRP composites", *J. Struct. Eng.*, **132**(1), 123-133.
- Mursi, M. and Uy, B. (2006a), "Behavior and design of fabricated high strength steel columns subjected to biaxial bending, Part 1: Experiments", *Adv. Steel Construct.*, **2**(4), 286-315.
- Mursi, M. and Uy, B. (2006b), "Behavior and design of fabricated high strength steel columns subjected to biaxial bending, Part 2: Analysis and design codes", *Adv. Steel Construct*, **2**(4), 316-354.
- Ozbakkaloglu, T. (2012), "Axial compressive behavior of square and rectangular high-strength concrete-filled FRP tubes", *J. Compos. Construct*, **17**(1), 151-161.
- Ozbakkaloglu, T. and Akin, E. (2011), "Behavior of FRP-confined normal- and high-strength concrete under cyclic axial compression", *J. Compos. Construct.*, **16**(4), 451-463.
- Ozbakkaloglu, T. and Fanggi, B.A.L. (2013), "Axial compressive behavior of FRP-concrete-steel double-skin tubular columns made of normal-and high-strength concrete", *J. Compos. Construct.*, **18**(1), 04013027.
- Ozbakkaloglu, T. and Oehlers, D.J. (2008), "Concrete-filled square and rectangular FRP tubes under axial compression", *J. Compos. Construct.*, **12**(4), 469-477.
- Ozbakkaloglu, T. and Saatcioglu, M. (2006), "Seismic behavior of high-strength concrete columns confined

- by fiber-reinforced polymer tubes”, *J. Compos. Construct.*, **10**(6), 538-549.
- Ozbakkaloglu, T. and Vincent, T. (2013), “Axial compressive behavior of circular high-strength concrete-filled FRP tubes”, *J. Compos. Construct.*, **18**(2), 04013037.
- Patel, V.I., Liang, Q.Q. and Hadi, M.N.S. (2015), “Biaxially loaded high-strength concrete-filled steel tubular slender beam-columns, Part II: Parametric study”, *J. Construct. Steel Res.*, **110**, 200-207.
- Yang, Z.J. (2010), “Behavior of high strength concrete filled square steel Tubes slender high columns with inner CFRP circular tube under bi-axial eccentric loading”, Master Thesis; Shenyang Jianzhu University, Shenyang, China.
- Yang, H., Lam, D. and Gardner, L. (2008), “Testing and analysis of concrete-filled elliptical hollow sections”, *Eng. Struct.*, **30**(12), 3771-3781.
- Yu, Z.W. and Ding, F.X. (2003), “Unified calculation method of compressive mechanical properties of concrete”, *J. Build. Struct.*, **24**(4), 41-46.
- Yu, T. and Teng, J.G. (2012), “Behavior of hybrid FRP-concrete-steel double-skin tubular columns with a square outer tube and a circular inner tube subjected to axial compression”, *J. Compos. Construct.*, **17**(2), 271-279.
- Yu, T., Wong, Y.L., Teng, J.G., Dong, S.L. and Lam, E.S. (2006), “Flexural behavior of hybrid FRP-concrete-steel double-skin tubular members”, *J. Compos. Construct.*, **10**(5), 443-452.
- Yu, T., Zhang, B., Cao, Y.B. and Teng, J.G. (2012), “Behavior of hybrid FRP-concrete-steel double-skin tubular columns subjected to cyclic axial compression”, *Thin-Wall. Struct.*, **61**, 196-203.
- Yu, T., Hu, Y.M. and Teng, J.G. (2014), “FRP-confined circular concrete-filled steel tubular columns under cyclic axial compression”, *J. Construct. Steel Res.*, **94**, 33-48.
- Zhang, B., Yu, T. and Teng, J.G. (2014), “Behavior of concrete-filled FRP tubes under cyclic axial compression”, *J. Compos. Construct.*, **19**(3), 04014060.
- Zhang, B., Teng, J.G. and Yu, T. (2015), “Experimental behavior of hybrid FRP-concrete-steel double-skin tubular columns under combined axial compression and cyclic lateral loading”, *Eng. Struct.*, **99**, 214-231.
- Zhu, M., Liu, J., Wang, Q. and Feng, X. (2010), “Experimental research on square steel tubular columns filled with steel-reinforced self-consolidating high-strength concrete under axial load”, *Eng. Struct.*, **32**(8), 2278-2286.